KT_KT100346 – 30.1.04/druckhaus köthen

C. H. M. Broeders, A. Yu. Konobeyev and A. A. Travleev

Calculation of the energy deposition in the targets from C to U irradiated with intermediate energy protons

The energy deposition was calculated for the targets from carbon to uranium irradiated with intermediate energy protons with the help of different models incorporated in the MCNPX code package (Bertini, CEM and ISABEL) and with the help of the CASCADE/INPE code. The values obtained using the different models and codes are in a good agreement for all targets except uranium. The comparison with the available experimental data for the heat deposition for 0.8, 1.0 and 1.2 GeV protons has been performed. The good agreement is observed for copper, lead and bismuth target. The best result is obtained with the help of the ISABEL model. The systematic dependence of the heat deposition from atomic number of the target was investigated. The contribution of different particles and energy ranges in the heat deposition has been studied at the primary proton energies from 0.3 to 2.5 GeV.

Berechnung von Energiefreisetzungen durch Bestrahlung mit Protonen mit Energien von 0.3 bis 2.5 GeV für Materialien von Kohlenstoff bis Uran. *Die Energiefreisetzung durch Bestrahlung mit Protonen mit Energien von 0.3 bis 2.5 GeV wurde systematisch berechnet mit den Codes MCNPX (Bertini, CEM und ISABEL Modelloptionen) und CASCADE/INPE. Die Ergebnisse dieser Rechnungen stimmen mit Ausnahme von Uran gut überein. Für die Energien 0.8, 1.0 und 1.2 GeV zeigen Vergleiche mit vorhandenen Experimenten gute Übereinstimmung, wobei die ISABEL Option des MCNPX Codes die besten Ergebnisse liefert. Der Beitrag der einzelnen Teilchen in den verschiedenen Energiebereichen auf die Energiefreisetzung wurde für primäre Proton-Energien von 0.3 bis 2.5 GeV analysiert.*

1 Introduction

The calculation of the energy deposition in materials is an important part of the computer simulation of materials properties under the irradiation with intermediate and high energy particles. The accuracy of such calculations is of paramount importance for the design study of the power sub-critical systems driven by proton accelerator (ADS).

The goal of this work is to analyze the heat deposition in the targets from carbon to uranium irradiated with intermediate energy protons, and compare the modern code calculations of the energy deposition with the experimental data.

The energy deposition has been calculated with the help of different models incorporated in the MCNPX package [1] and with the help of the CASCADE/INPE code [2]. The contribution of different particles and energy ranges in the heat depositions has been studied. The comparison with the experimental data allows estimating the error value of the heat deposition calculations for the ADS systems of different types and for the other applications.

For the comparison with the code predictions, the experimental data for the heat deposition obtained for thick cylindrical targets in Refs. [3–6] have been used. Formerly, these data [3–6] were compared with the LAHET code calculations in Ref. [7]. Since the publication [7] the models and algorithms describing the nucleon-nucleus interactions in the MCNPX code were noticeably improved. Especially it concerns the extension of the evaluated nuclear data files up to 150 MeV for a number of nuclides [8], providing the most accurate description of the particle transport at these energies. The comparison of the modern codes with available experimental data seems to be opportune and urgent.

2 Brief description of the models and codes used for the energy deposition calculation

The calculation of the energy deposition has been performed with the help of the various models incorporated in the MCNPX code package [1]: the Bertini model, the ISABEL model and the CEM model. Also, the calculations were done with the help of the CASCADE/INPE code [2] which includes the original high energy particle transport code and MCNP/4C code [9].

2.1 The MCNPX code

All three intranuclear cascade models included in the MCNPX code (Bertini, CEM and ISABEL) use the same data set to describe the particle transport in a matter.

Historically, the development of the Bertini model [10, 11] was linked with the widely used NMTC code and the HETC code operation. The ISABEL model [12, 13] is the further development of the approach of K. Chen, Z. Fraenkel, G. Friedlander et al. [14] which was put in the basis of the VEGAS code. The popular CEM model has being created and improved during last three decades [15–19].

The main difference between all three models incorporated in the MCNPX code is the approach used for the intranuclear interaction simulation, determination of the point of particle interaction, selection of collision partners for the moving nucleons and pions and the parameterization of n-n and π-n cross-sections. The common feature for all models is the approximation of the real nuclear density distribution by the concentric zones with the constant density. The use of this approximation raises the question about the necessity to take

into account or not the refraction and the reflection of the momentum of nucleon crossing the zone boundary. The consideration of such effects is more physically based [20] but results in the worse agreements with the experimental angular nucleon distributions [21]. Following the recommendations from Ref. [1] the reflection and the refraction of nucleons on the zone boundaries were not considered in the present calculations with the help the Bertini model, the ISABEL model and the CEM model.

The next stage of the reaction followed the emission of fast particles is the pre-equilibrium stage described by the exciton model. The addition of this stage noticeably compensates the lack of the approach neglecting the refraction and the reflection of nucleon momentum at the boundaries of the nuclear zones. Such consideration allows getting the satisfactory description of the nucleon angular distributions not only at the small emission angles due to the absence of the refraction/reflection, but also at the relatively big angles of the nucleon emission.

The final stage of the reaction is the evaporation described on the basis of the Weisskopf-Ewing approach. The Fermi gas model with the different set of nuclear level density parameters is used to describe the level density of the excited nuclei in all intranuclear cascade evaporation models incorporated in the MCNPX code.

The stopping power for protons and other charged nuclear reaction products are calculated with the help of the module used in the LAHET Code System and modified as described in Ref. [27].

2.2 The CASCADE/INPE code

The CASCADE/INPE code has being developed and improved during the last decades [2, 15, 16, 22, 23]. The model for the simulation of the intranuclear cascade nucleon and meson interactions is quite different from the models incorporated in the MCNPX package. The detail description is given in Ref. [22]. The main features of the model are the consideration of the time coordinate, the use of the realistic nuclear density with the diffuse boundary and the description of the change in the nuclear density during the fast particle emission. The pre-equilibrium stage of the reaction describing by the exciton model is not considered in the present calculations. After the finish of the fast particle emission the evaporation stage occurs.

To describe the non-equilibrium α-particle emission from an excited nucleus the coalescence model from Refs. [24, 25] is used.

The Fermi gas model with level density parameter equal to A/10 is used to calculate the nuclear level density for the excited nuclei. The general expressions describing the particle evaporation widths in the CASCADE/INPE model and in the CEM model are the same. The fission channel is described according to Ref. [26].

The creation and the emission of the following particles have been simulated in the present work with the help the MCNPX code and the CASCADE/INPE code: neutrons, protons, deuterons, tritons, ^{3}He, α-particles, charged pions π^+, π, neutral pions and photons.

2.3 Use of the evaluated nuclear data files for low energy particle transport calculation

Data from ENDF/B-VI (Release 8) library were used for the particle transport calculations with the MCNPX code at low energies. The evaluated data up to 150 MeV from ENDF/B-VI (8) were applied for the energy deposition calculations for carbon, aluminum, iron, copper, lead and bismuth. For uranium the available data up to 20 MeV were used.

For the systematic calculation of the energy deposition (Chapter 4.1) the neutron data for the nuclides with Z = 3–92, which are absent in ENDF/B-VI (8), were taken from other nuclear data libraries at the energies below 20 MeV. For ^{nat}Zn data were taken from JEFF-3.0 (original data from BROND-2.2), for ^{70}Ge, ^{162}Er, ^{164}Er, ^{168}Er, and ^{170}Er the JENDL-3.3 data were adopted, for ^{nat}Pt data were taken from JEFF-3.0 (original data from ENDL-78).

The low energy neutron transport calculations with the help of the CASCADE/INPE code were also based on the ENDF/B-VI (8) data. The photon transport was treated with the help of the MCNP/4C code. The protons and other particles were tracked with the help of the theoretical models.

3 Experimental data for the heat deposition

The heat deposition has been measured in Refs. [3–6] for two cylindrical targets with radius equal to 5 and 10 cm and height equal to 60 cm irradiated with 0.8, 1.0 and 1.2 GeV protons. The data were obtained for protons impinging on the butt-end of the cylinder with the Gaussian radial distribution with a full width at half-maximum equal to 2.4 cm.

The most detailed data were obtained for the target with the radius R = 10 cm [3–6]. The data for this target is used for the comparison of the experimental data and the code calculations in the present work.

The experimental values of the total heat deposition for the carbon, aluminum, iron and copper targets were obtained by the integration of the linear density of the energy deposition (dQ/dz) along the beam axis measured in Refs. [5, 6]. Data for lead and bismuth were taken from Ref. [3] and for uranium from Ref. [7].

4 Results

4.1 The total values of the heat deposition

The calculated and measured values of the total heat deposition (Q) are presented in Figs. 1–7 for carbon, aluminum, iron, copper, lead, bismuth and uranium. Data correspond to the cylindrical target with the radius equal to 10 cm. Figs. 5–7 show also the values of the heat deposition obtained with the help of the LAHET code in Ref. [7].

There is a rather good agreement between predictions of different models and codes except the calculations for uranium (Fig. 7). For uranium the values of Q calculated with the help of the CEM model and the CASCADE/INPE model are close. The ISABEL model predictions are in the agreement with the Bertini model, but not with the CEM model and the CASCADE/INPE model. The origin of the difference is the use of the different approaches to describe the fission-evaporation competition in the models.

As compared with the experimental data, the calculation overestimates the heat deposition for carbon (Fig. 1) and underestimates for aluminum and iron (Figs. 2, 3). There is a good agreement between the experimental and calculated values of the heat deposition for copper (Fig. 4). For lead, bismuth and uranium the results of the calculations are rather higher than the measured values of Q. The deviation of the experimental data and calculated values increases for carbon and bismuth with the proton energy growth, For aluminum,

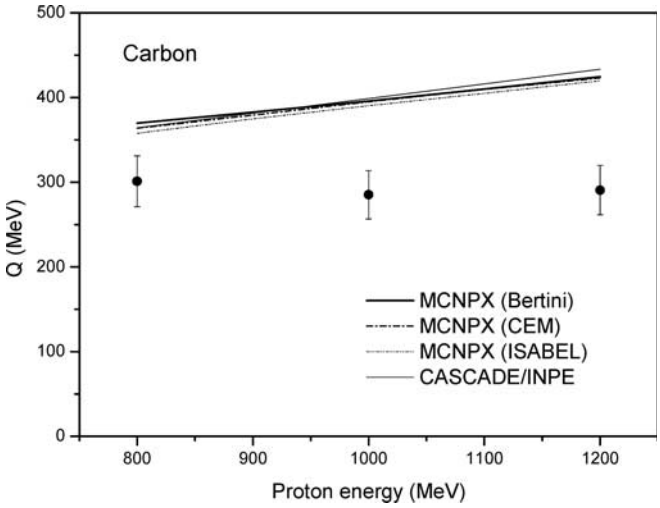

Fig. 1. Total heat deposition in the carbon target calculated with the help of the MCNPX code using the Bertini model (thick solid line), the CEM model (dash-dot line), the ISABEL model (dot line) and with the help of the CASCADE/INPE code (thin solid line). The experimental data (black circle) are from Ref. [5].

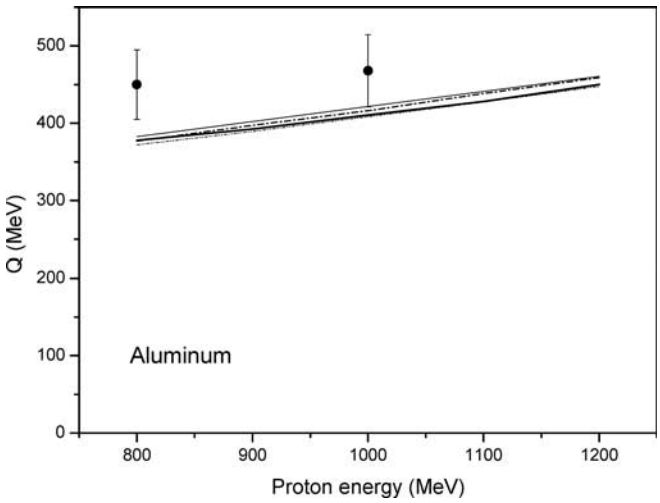

Fig. 2. Total heat deposition in the aluminum target. The experimental data are from Ref. [5]. The symbols are as in Fig. 1.

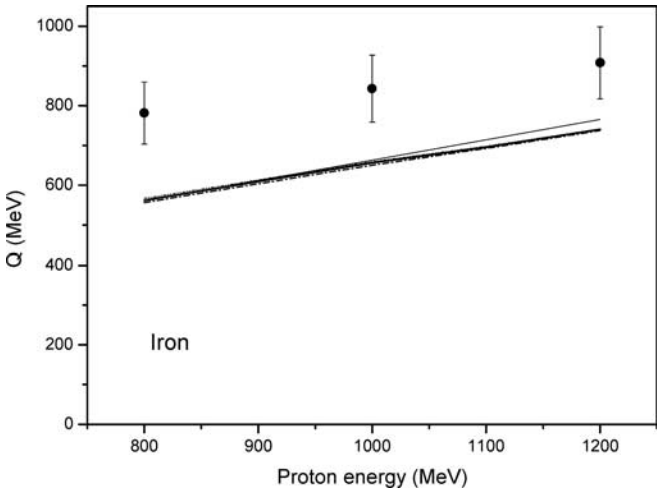

Fig. 3. Total heat deposition in the iron target. The experimental data are from Ref. [6]. The symbols are as in Fig. 1.

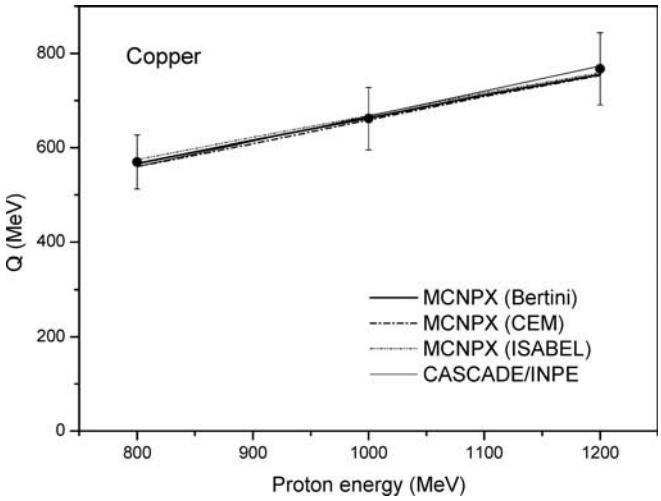

Fig. 4. Total heat deposition in the copper target. The experimental data are from Ref. [6]. The symbols are as in Fig. 1.

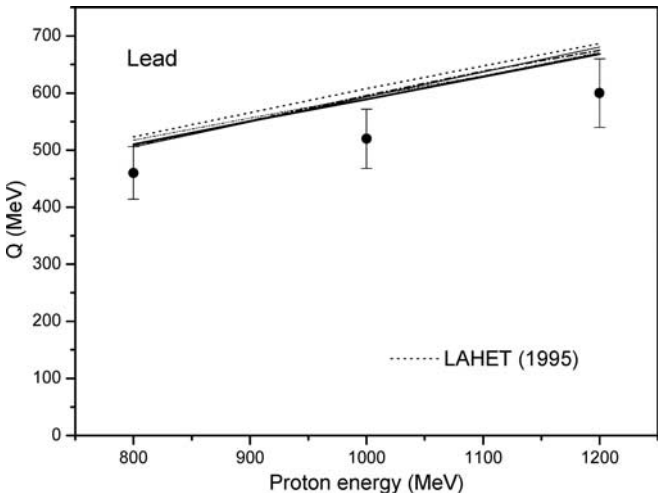

Fig. 5. Total heat deposition in the lead target calculated with the help of the MCNPX code, the CASCADE/INPE code and the LAHET code (dashed line). The experimental data are from Ref. [3]. The symbols are as in Fig. 1.

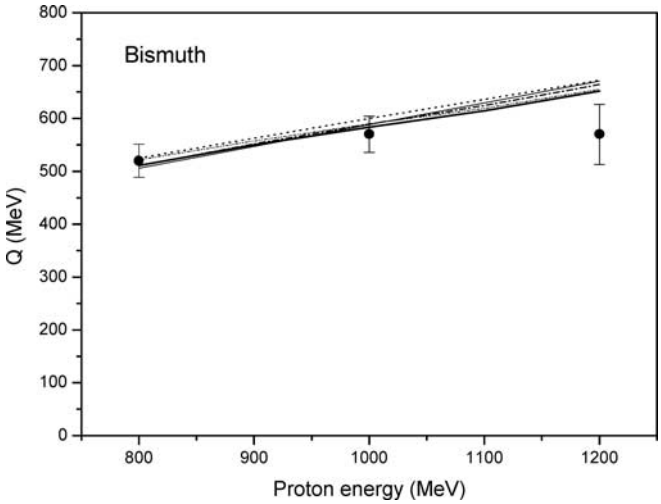

Fig. 6. Total heat deposition in the bismuth target. The experimental data are from Ref. [3]. The symbols are as in Figs. 1 and 5.

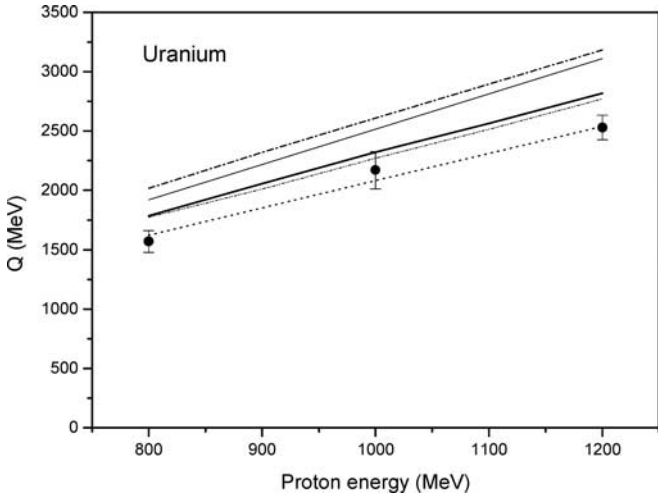

Fig. 7. Total heat deposition in the uranium target. The experimental data are from Ref. [4, 7]. The symbols are as in Figs. 1 and 5.

iron and lead one may say about "energy independent" discrepancy. The LAHET code calculation has the maximal deviation from the experimental values for lead and bismuth (Figs. 5, 6) and shows the best result for uranium (Fig. 7).

The values describing the deviation of the experimental data and the MCNPX code and the CASCADE/INPE code calculations are given in Table 1.

According to the data from Table 1, the Bertini model gives the best description of the experimental data for copper, lead and bismuth. The ISABEL model provides the best result for carbon and uranium. The CASCADE/INPE calculations have the minimal error for aluminum and iron. Formally, for all seven elements the ISABEL model gives the best description of the measured data (last row in Table 1). At the same time the error values shown in Table 1 for different codes are rather close (14.2 to 17) and the use of any code does not give the substantial gain in the experimental data description comparing with other codes.

To understand better the general character of the difference between the calculated values and the experimental data the calculations have been performed for a wide number of the elements irradiated with intermediate energy protons. The energy deposition has been calculated for seventy natural mixtures of isotopes with atomic number from Z = 3 to 92 except gases. The target was the cylinder with radius equal to 10 cm and the height equal to 60 cm, for which the measurement of the heat deposition was performed in Refs. [3–6]. Fig. 8 shows the results of the calculation performed with the help of the Bertini model and the measured values of the energy deposition for the proton energy equal to 0.8 GeV and 1.2 GeV. The statistical error of the Monte Carlo calculations does not exceed 1 % for all elements considered.

Fig. 8 shows that the general dependence of Q is not monotonous function of the atomic number Z. The holes correspond to the alkali elements Li, Na, K, Rb and Cs which have the maximal values of the proton ranges and also to lead and bismuth. The calculated values of Q are in a general agreement with the experimental values of the heat deposition for all cases except iron. The measured heat deposition is noticeably higher then the values of Q calculated for iron and neighboring elements. It should be noted that for 800 MeV protons the measured value of the heat deposition for iron (Q = 780 MeV) is peculiarly close to the primary proton energy.

Table 1. The error between the calculated and measured values of the heat deposition (%), calculated as follows $(1/N)\Sigma|Q_i^{exp} - Q_i^{calc}|/Q_i^{exp}$. *The minimal value for each target is marked out.*

Target	Proton energy (MeV)	MCNPX			CASCADE/ INPE
		Bertini model	CEM model	ISABEL model	
Carbon	800	22.8	20.7	18.8	20.9
	1 000	38.8	38.5	36.8	39.8
	1 200	46.0	45.5	44.4	49.0
	all energies	35.9	34.9	33.3	36.6
Aluminum	800	16.0	16.2	17.3	15.0
	1 000	12.2	11.1	12.7	9.9
	all energies	14.1	13.6	15.0	12.4
Iron	800	28.1	28.8	27.5	28.2
	1 000	22.1	22.9	21.8	21.3
	1 200	18.5	18.8	18.4	15.7
	all energies	22.9	23.5	22.5	21.8
Copper	800	0.7	1.7	0.9	1.6
	1 000	0.2	0.5	0.9	0.8
	1 200	1.6	1.8	1.1	0.8
	all energies	0.8	1.3	1.0	1.1
Lead	800	10.8	10.4	12.5	9.9
	1 000	13.3	14.5	14.2	14.0
	1 200	11.4	12.5	11.8	13.4
	all energies	11.8	12.5	12.8	12.4
Bismuth	800	1.7	1.8	0.3	2.7
	1 000	2.4	3.4	3.5	3.2
	1 200	14.4	16.5	15.0	17.7
	all energies	6.1	7.2	6.3	7.9
Uranium	800	13.7	28.5	12.9	22.3
	1 000	7.0	20.3	4.6	15.9
	1 200	11.4	25.8	9.5	23.0
	all energies	10.7	24.9	9.0	20.4
All targets		14.7	17.0	14.2	16.3

4.2 The linear density of the heat deposition

The linear density of the energy deposition along the target axis calculated and measured for the target with R = 10 cm and H = 60 cm is shown in Figs. 9–20. The calculations were performed with the help of the MCNPX code using the Bertini model, the CEM model and the ISABEL model and with the help of the CASCADE/INPE code. Figs. 9–20 show the results obtained for 0.8 GeV, 1.0 GeV (for Al) and 1.2 GeV protons and the values of the heat deposition measured in Refs. [3, 5, 6].

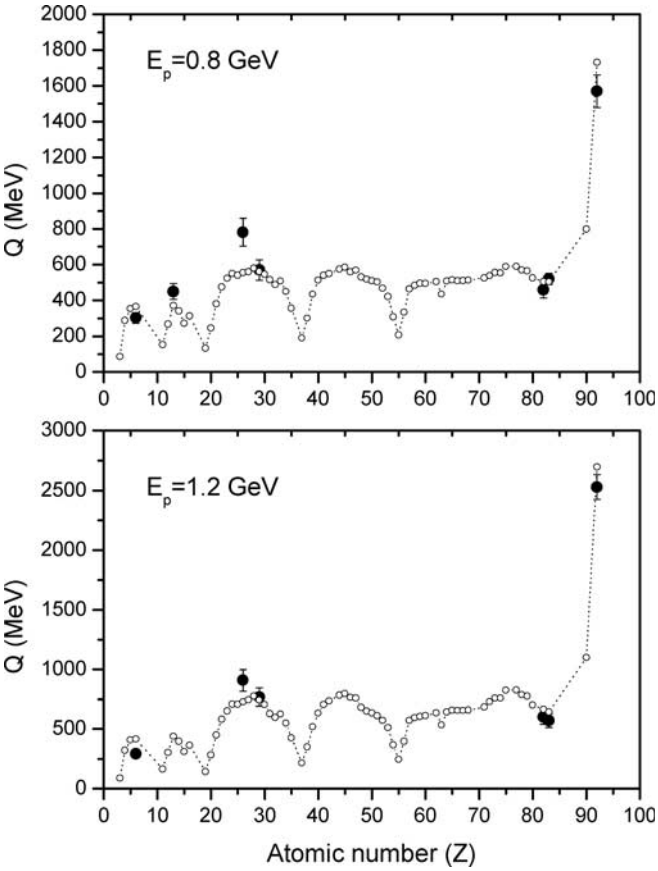

Fig. 8. Total heat deposition in the cylindrical target (R = 10 cm, H = 60 cm) calculated with the help of the Bertini model and the MCNPX code (open circle) for natural mixtures of isotopes from Li to U at the energy of primary protons equal to 0.8 and 1.2 GeV. The experimental data (black circle) are from Ref. [3–6].

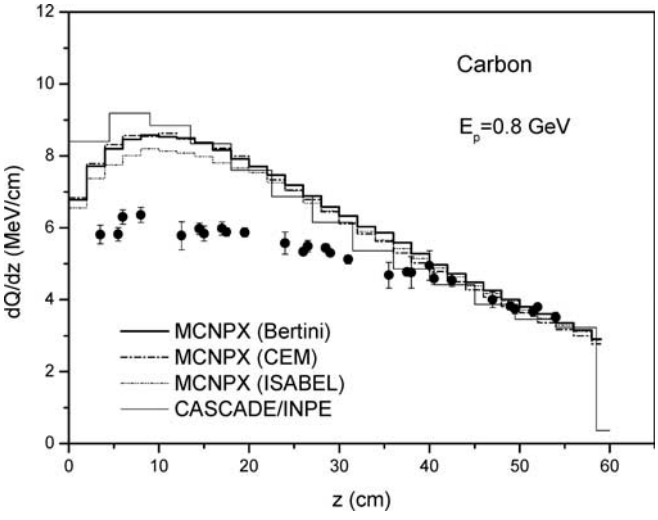

Fig. 9. Energy deposition in the carbon target irradiated with 0.8 GeV protons calculated with the help of the MCNPX code using the Bertini model (thick solid line), the CEM model (dash-dot line), the ISABEL model (dot line) and with the help of the CASCADE/INPE code (thin solid line). The experimental data (black circle) are from Ref. [5].

The noticeable deviation of the calculated and measured values of the heat deposition is for carbon (Figs. 9, 10) at the distance up to 30–40 cm from the point of the beam penetration along the target axis. For aluminum the calculated values of Q are lower than the measured ones for a whole target length (Figs. 11, 12). The substantial difference between the

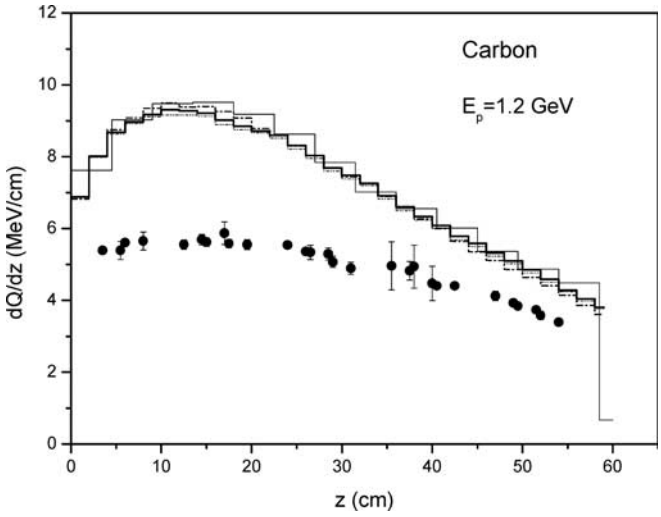

Fig. 10. Energy deposition in the carbon target irradiated with 1.2 GeV protons. The experimental data are from Ref. [5]. The symbols are as in Fig. 9.

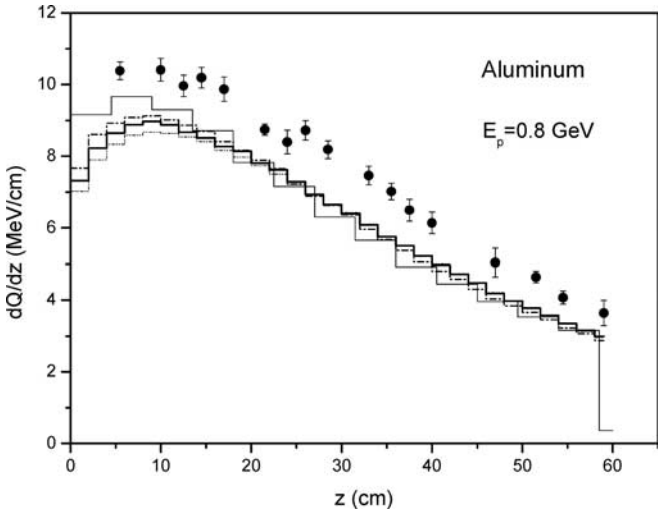

Fig. 11. Energy deposition in the aluminum target irradiated with 0.8 GeV protons. The experimental data are from Ref. [5]. The symbols are as in Fig. 9.

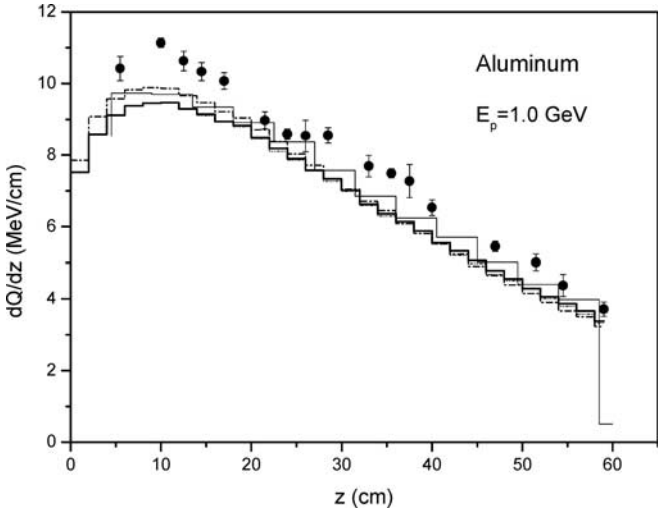

Fig. 12. Energy deposition in the aluminum target irradiated with 1.0 GeV protons. The experimental data are from Ref. [5]. The symbols are as in Fig. 9.

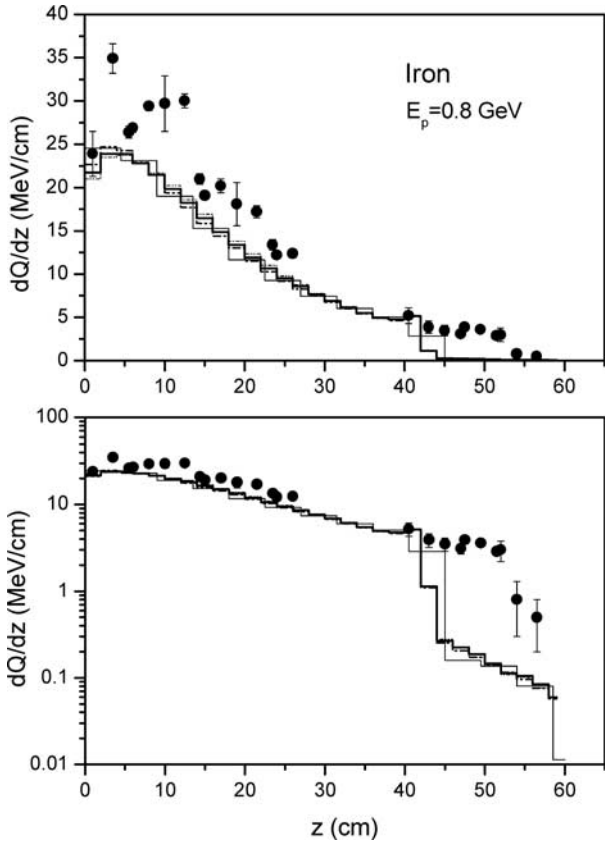

Fig. 13. Energy deposition in the iron target irradiated with 0.8 GeV protons. The experimental data are from Ref. [6]. The symbols are as in Fig. 9.

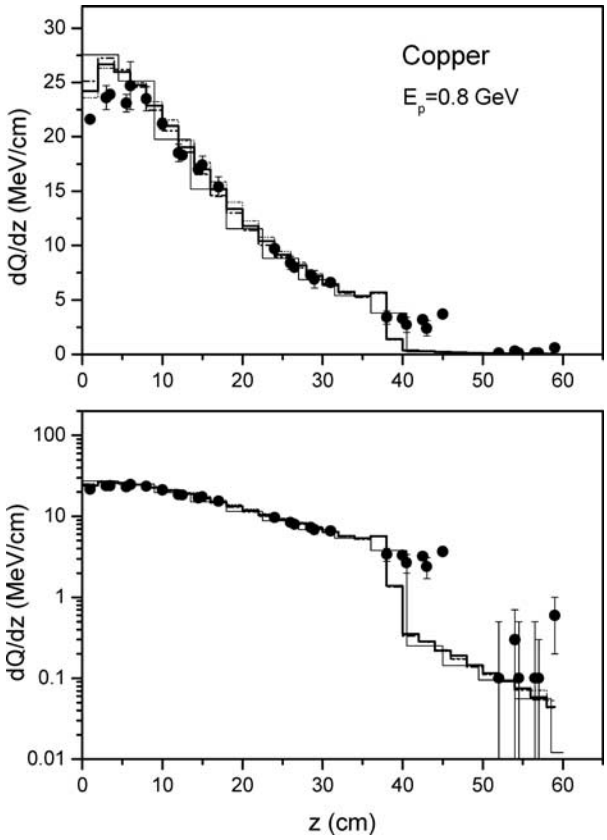

Fig. 15. Energy deposition in the copper target irradiated with 0.8 GeV protons. The experimental data are from Ref. [6]. The symbols are as in Fig. 9.

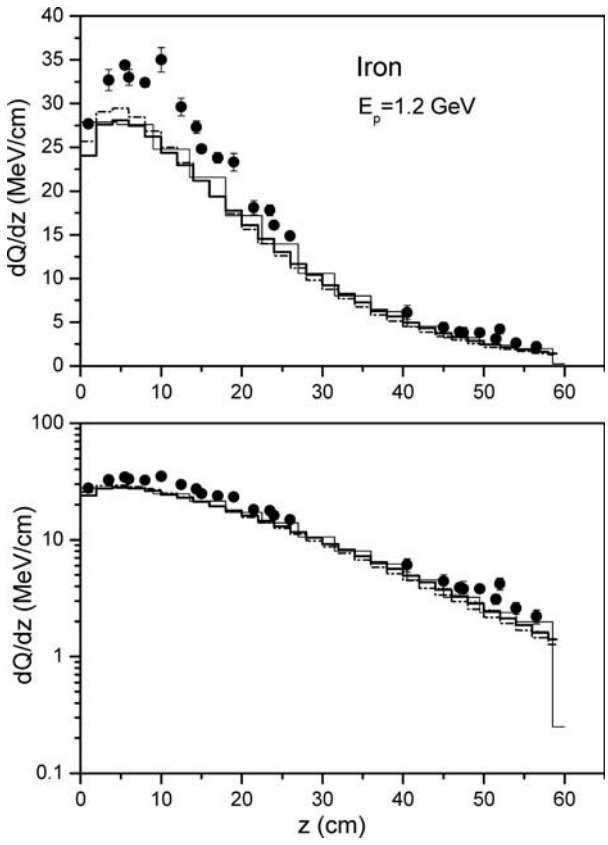

Fig. 14. Energy deposition in the iron target irradiated with 1.2 GeV protons. The experimental data are from Ref. [6]. The symbols are as in Fig. 9.

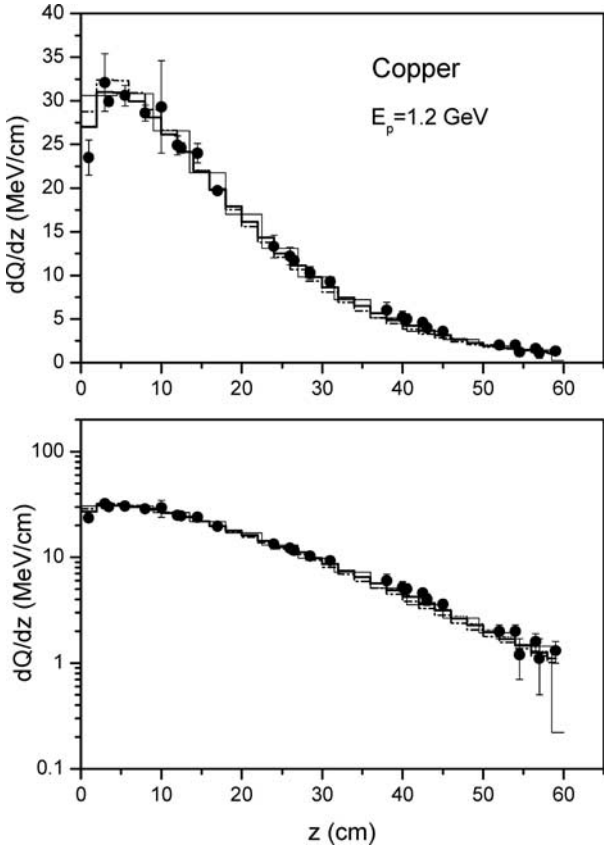

Fig. 16. Energy deposition in the copper target irradiated with 1.2 GeV protons. The experimental data are from Ref. [6]. The symbols are as in Fig. 9.

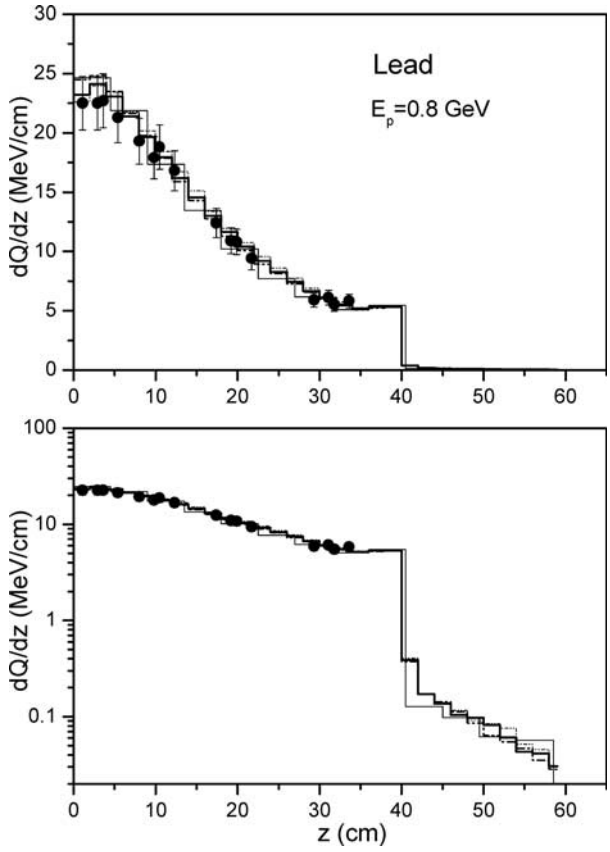

Fig. 17. Energy deposition in the lead target irradiated with 0.8 GeV protons. The experimental data are from Ref. [3]. The symbols are as in Fig. 9.

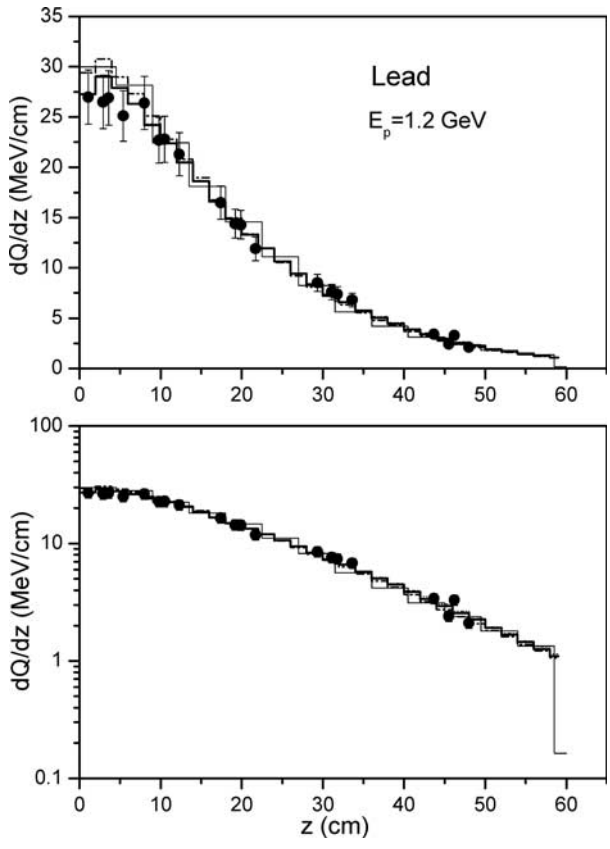

Fig. 18. Energy deposition in the lead target irradiated with 1.2 GeV protons. The experimental data are from Ref. [3]. The symbols are as in Fig. 9.

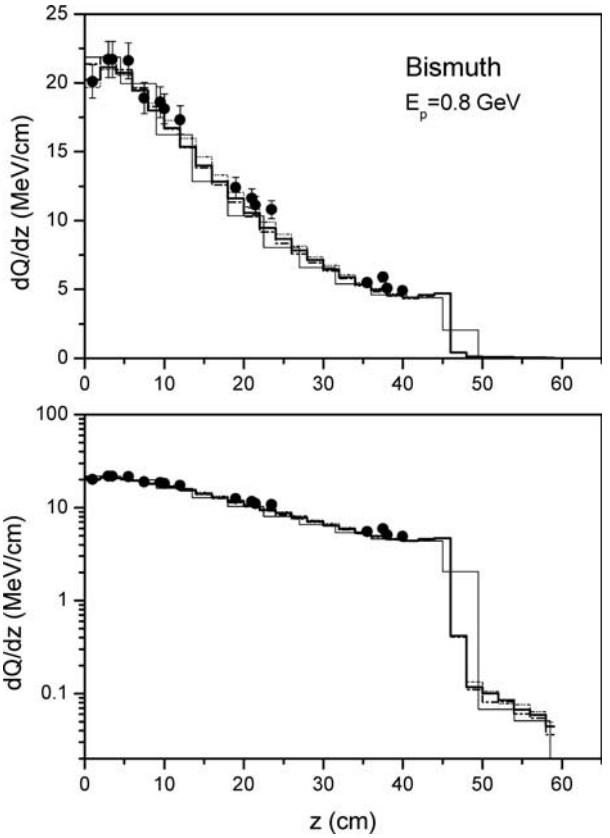

Fig. 19. Energy deposition in the bismuth target irradiated with 0.8 GeV protons. The experimental data are from Ref. [3]. The symbols are as in Fig. 9.

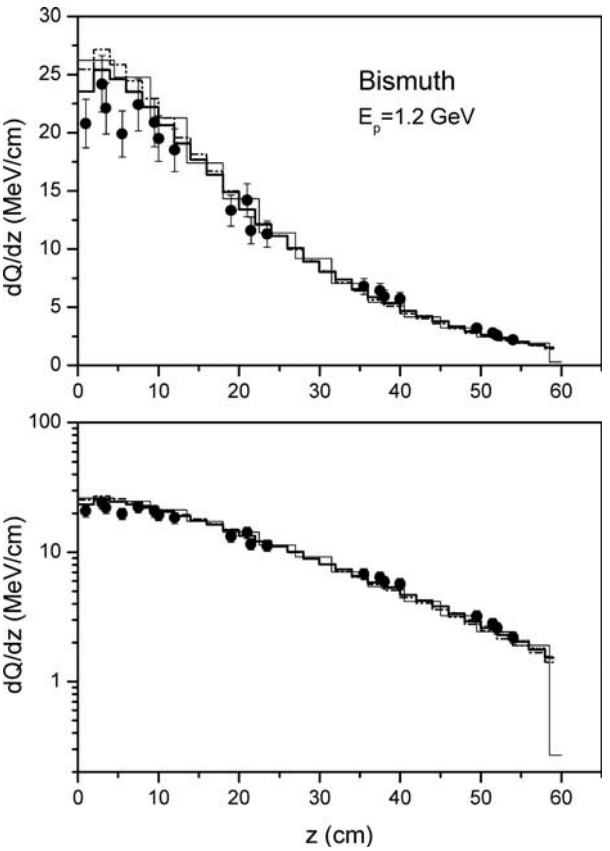

Fig. 20. Energy deposition in the bismuth target irradiated with 1.2 GeV protons. The experimental data are from Ref. [3]. The symbols are as in Fig. 9.

Table 2. Energy deposition (MeV) in the cylindrical iron target (R = 10 cm, H = 60 cm) irradiated with 0.8 GeV protons calculated with the help of the different models. (Empty cell means that the contribution is not identified)

Value	MCNPX			CASCADE/INPE
	Bertini model	CEM model	ISABEL model	
Total	561.29 (100.0 %)	555.85 (100.0 %)	566.21 (100.0 %)	561.81 (100.0 %)
Ionization from primary proton	238.69 (42.53)	238.69 (42.94)	238.69 (42.16)	252.70 (44.98)
Ionization from secondary protons	250.29 (44.59)	233.91 (42.08)	258.02 (45.57)	220.30 (39.21)
Photon interactions	41.00 (7.31)	40.18 (7.23)	40.98 (7.24)	34.64 (6.17)
photons formed from π^0 decay	21.75 (3.87)	21.45 (3.86)	23.51 (4.15)	17.28 (3.08)
Charged pions (π^+, π^-)	10.52 (1.87)	10.24 (1.84)	11.16 (1.97)	25.23 (4.49)
negative pions, (π^-)				2.51 (0.45)
Ionization from light clusters (d, t, ^{3}He, α)	11.26 (2.01)	22.16 (3.99)	9.24 (1.63)	17.37 (3.09)
deuterons	5.35 (0.95)	11.02 (1.98)	4.40 (0.78)	2.51 (0.45)
tritons	0.57 (0.10)	2.96 (0.53)	0.41 (0.07)	0.56 (0.10)
^{3}He	0.36 (0.06)	2.39 (0.43)	0.20 (0.03)	0.50 (0.09)
α-particles	4.98 (0.89)	5.78 (1.04)	4.23 (0.75)	13.80 (2.46)
non-equilibrium α-particles				7.58 (1.35)
Total recoils	9.52 (1.70)	10.67 (1.92)	8.12 (1.43)	11.57 (2.06)
recoils from neutron induced reactions	3.01 (0.54)	3.09 (0.56)	2.75 (0.48)	2.89 (0.51)

Table 3. Energy deposition (MeV) in the cylindrical iron target (R = 10 cm, H = 60 cm) irradiated with 1.2 GeV protons calculated with the help of the different models. (Empty cell means that the contribution is not identified)

Value	MCNPX			CASCADE/INPE
	Bertini model	CEM model	ISABEL model	
Total	739.15 (100.0 %)	737.57 (100.0 %)	740.43 (100.0 %)	765.31 (100.0 %)
Ionization from primary proton	198.94 (26.91)	198.94 (26.97)	198.94 (26.87)	208.90 (27.30)
Ionization from secondary protons	379.10 (51.29)	352.68 (47.82)	382.06 (51.60)	358.72 (46.87)
Photon interactions	91.29 (12.35)	94.39 (12.80)	91.65 (12.38)	85.91 (11.23)
photons formed from π^0 decay	60.11 (8.13)	64.71 (8.77)	61.87 (8.36)	56.99 (7.45)
Charged pions (π^+, π^-)	30.88 (4.18)	31.06 (4.21)	31.27 (4.22)	63.96 (8.36)
negative pions, (π^-)				8.92 (1.17)
Ionization from light clusters (d, t, ^{3}He, α)	21.08 (2.85)	40.97 (5.55)	19.61 (2.65)	34.02 (4.45)
deuterons	10.18 (1.38)	19.33 (2.62)	9.64 (1.30)	5.16 (0.67)
Tritons	1.31 (0.18)	6.02 (0.82)	1.19 (0.16)	1.26 (0.16)
^{3}He	0.97 (0.13)	5.05 (0.68)	0.87 (0.12)	1.13 (0.15)
α-particles	8.63 (1.17)	10.57 (1.43)	7.91 (1.07)	26.47 (3.46)
non-equilibrium α-particles				14.18 (1.85)
Total recoils	17.85 (2.42)	19.53 (2.65)	16.89 (2.28)	13.79 (1.80)
recoils from neutron induced reactions	5.17 (0.70)	5.20 (0.70)	4.96 (0.67)	5.46 (0.71)

Table 4. Energy deposition (MeV) in the cylindrical lead target (R = 10 cm, H = 60 cm) irradiated with 0.8 GeV protons calculated with the help of the different models. (Empty cell means that the contribution is not identified)

Value	MCNPX			CASCADE/INPE
	Bertini model	CEM model	ISABEL model	
Total	510.49 (100.0 %)	510.52 (100.0 %)	519.44 (100.0 %)	507.19 (100.0 %)
Proton interactions(*)	441.48 (86.48)	432.75 (84.77)	454.48 (87.49)	429.56 (84.69)
ionization from primary protons	260.46 (51.02)	260.46 (51.02)	260.46 (50.14)	260.35 (51.33)
fission induced by protons				8.51 (1.68)
Photon interactions	45.13 (8.84)	43.89 (8.60)	43.74 (8.42)	40.23 (7.93)
photons produced in neutron in-duced reactions below 20 MeV				16.93 (3.34)
photons formed from π^0 decay	18.28 (3.58)	17.78 (3.48)	18.29 (3.52)	13.22 (2.61)
Charged pions (π^+, π^-)	7.80 (1.53)	7.52 (1.47)	6.97 (1.34)	16.97 (3.35)
negative pions, (π^-)				2.15 (0.42)
fission induced by pions				0.10 (0.02)
Ionization from light clusters (d, t, ^{3}He, α)	14.36 (2.81)	24.69 (4.84)	12.53 (2.41)	18.67 (3.68)
deuterons	3.42 (0.67)	13.87 (2.72)	2.82 (0.54)	2.39 (0.47)
tritons	1.54 (0.30)	4.10 (0.80)	1.24 (0.24)	1.22 (0.24)
^{3}He	0.11 (0.02)	2.15 (0.42)	0.07 (0.01)	0.18 (0.04)
α-particles	9.28 (1.82)	4.58 (0.90)	8.40 (1.62)	14.88 (2.93)
non-equilibrium α-particles				7.75 (1.53)
Neutron interactions (**)	1.71 (0.34)	1.67 (0.33)	1.73 (0.33)	1.76 (0.35)
fission induced by neutrons				0.46 (0.09)
Fission				9.08 (1.79)

(*) including ionization, fission and recoils induced by primary and secondary protons
(**) including fission and recoils

measured and calculated energy deposition is for iron at the distance z > 5 cm (Figs. 13, 14). The most relative deviation is for 0.8 GeV protons at the distance z exceeding the proton range (R_p) in iron equal to 42.3 cm (Fig. 13). There is a quite good agreement between measurements and calculations for the copper target for a whole target length (Figs. 15, 16) except the distance z = 40–45 cm for 0.8 GeV protons (Fig. 15) which is close to the proton range in copper, R_p = 38.8 cm. There is a good agreement between different code calculations and the experimental data for the lead and bismuth target (Figs. 17–20). The Q(z) dependence for 0.8 GeV protons shows the weak growth at the distance close to proton ranges in the targets (Figs. 13, 15, 17, 19). It is due to the sharp rise of the proton stopping power in this region and the presence of the relatively small part of the primary protons not undergoing the nuclear interactions. For the carbon and aluminum targets and for all targets at 1.2 GeV proton energy the range of protons exceeds the target length.

4.3 The contribution of different particles and energy ranges to the heat deposition

The contribution of the different particles and energy regions to the total value of the energy deposition has been studied for the different targets with the help of the MCNPX code and the CASCADE/INPE code.

Tables 2 and 3 show the calculated contributions of the different physical processes in the heat deposition in the iron target irradiated with 0.8 and 1.2 GeV protons. It is seen that the principal contribution to the total heat deposition is due to the ionization from the primary and secondary protons and photon interactions with the matter. With the growth of the initial proton energy the contribution of the primary protons decreases. The part of other particles is growing.

The good agreement is observed for different code calculations for the contribution of the ionization from primary and secondary protons and photon interactions including the photons produced from the π^0 decay. The contribution of the ionization from the light clusters (d, t, ^{3}He, α) are close for both the Bertini model and the ISABEL model and for the CEM model and the CASCADE/INPE model. At the same time the separate contribution of deuterons, tritons, ^{3}He and α-particles are different for the CEM model and the CASCADE/INPE model calculations. The calculated contribution of charged pions is in a good agreement for the Bertini, CEM and ISABEL models. The result of the CASCADE/INPE code is twice more than the

other code calculations. The energy released by the heavy recoils calculated with the help of the different codes is similar.

The contribution of different physical processes to the heat deposition in the lead target is shown in Tables 4 and 5. The principal contributors are the proton and photon interactions,

Table 5. Energy deposition (MeV) in the cylindrical lead target (R = 10 cm, H = 60 cm) irradiated with 1.2 GeV protons calculated with the help of the different models. (Empty cell means that the contribution is not identified)

Value	MCNPX			CASCADE/INPE
	Bertini model	CEM model	ISABEL model	
Total	665.93 (100.0 %)	676.53 (100.0 %)	668.71 (100.0 %)	685.66 (100.0 %)
Proton interactions(*)	511.76 (76.85)	502.56 (74.29)	516.24 (77.20)	499.50 (72.85)
ionization from primary protons	223.92 (33.62)	223.92 (33.10)	223.92 (33.49)	218.58 (31.88)
fission induced by protons				12.40 (1.81)
Photon interactions	93.66 (14.07)	94.22 (13.93)	93.53 (13.99)	89.79 (13.10)
photons produced in neutron in-duced reactions below 20 MeV				29.50 (4.30)
photons formed from π^0 decay	48.37 (7.26)	51.35 (7.59)	49.17 (7.35)	44.01 (6.42)
Charged pions (π^+, π^-)	22.93 (3.44)	22.76 (3.36)	22.41 (3.35)	44.59 (6.50)
negative pions, (π^-)				8.12 (1.18)
fission induced by pions				0.47 (0.07)
Ionization from light clusters (d, t, ^{3}He, α)	34.45 (5.17)	54.02 (7.98)	33.41 (5.00)	48.30 (7.04)
deuterons	8.89 (1.33)	28.68 (4.24)	8.64 (1.29)	6.29 (0.92)
tritons	4.59 (0.69)	9.97 (1.47)	4.41 (0.66)	3.49 (0.51)
^{3}He	0.62 (0.09)	5.75 (0.85)	0.60 (0.09)	0.61 (0.09)
α-particles	20.35 (3.06)	9.62 (1.42)	19.77 (2.96)	37.91 (5.53)
non-equilibrium α-particles				19.50 (2.84)
Neutron interactions (**)	3.12 (0.47)	2.96 (0.44)	3.11 (0.47)	3.48 (0.51)
fission induced by neutrons				1.13 (0.16)
Fission				14.00 (2.04)

(*) including ionization, fission and recoils induced by primary and secondary protons
(**) including fission and recoils

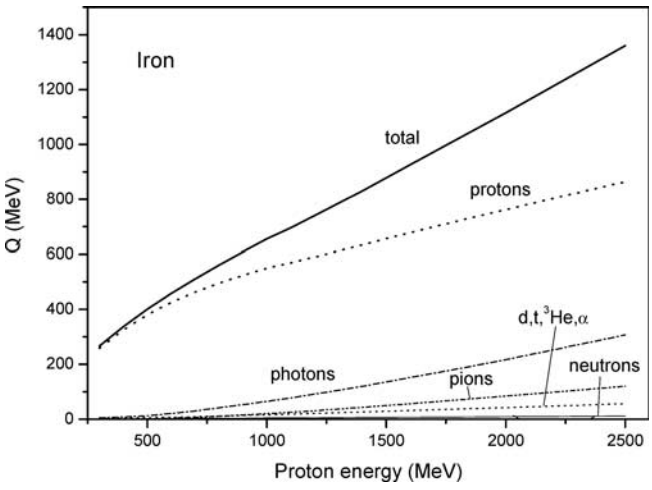

Fig. 21. Absolute contribution of different particles in the heat deposition in the iron target irradiated with intermediate energy protons. "Neutrons" means the contribution of recoils produced in the neutron induced reactions.

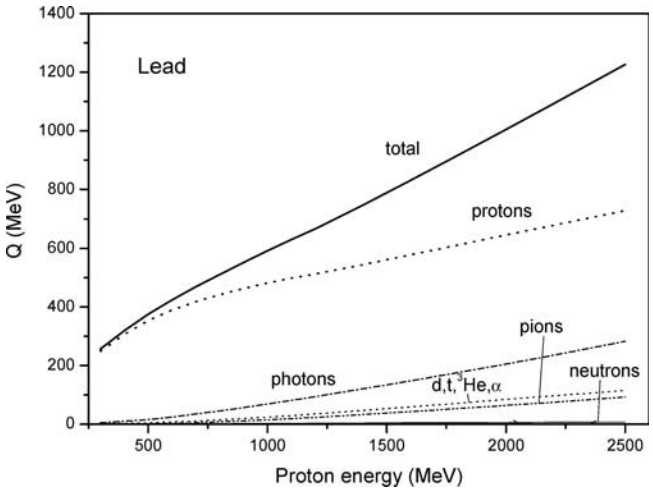

Fig. 22. Absolute contribution of different particles in the heat deposition in the lead target irradiated with intermediate energy protons. "Neutrons" means the contribution of neutron induced fission and recoils.

the same as for the iron target. The different codes predict the close values of Q for the ionization of primary protons, for the photon and neutron interactions. As for the iron target the CASCADE/INPE code predicts more charged pions than the models included in the MCNPX code. The energy deposited by the ionization from the light clusters is close for the Bertini model and the ISABEL model and for the CEM model and the CASCADE/INPE model.

Figs. 21–23 show the contribution of the interactions of different particles in the total heat deposition for the iron and lead targets at the energies of primary protons from 0.3 to 2.5 GeV. The calculations are performed with the help of the Bertini model and the MCNPX code for the cylindrical target (R = 10 cm, H = 60 cm). The absolute values of the different contributions are shown in Figs. 21 and 22 and the relative values are presented in Fig. 23. One can see the decrease of the relative contribution of the proton interactions in the energy deposition and the increase of other contributions with the primary particle energy growing.

Figs. 24–30 show the relative contribution of different energy range of protons, photons and pions in the heat deposition calculated for the iron and lead targets. Here the relative values correspond to the ratio of the heat deposition from the

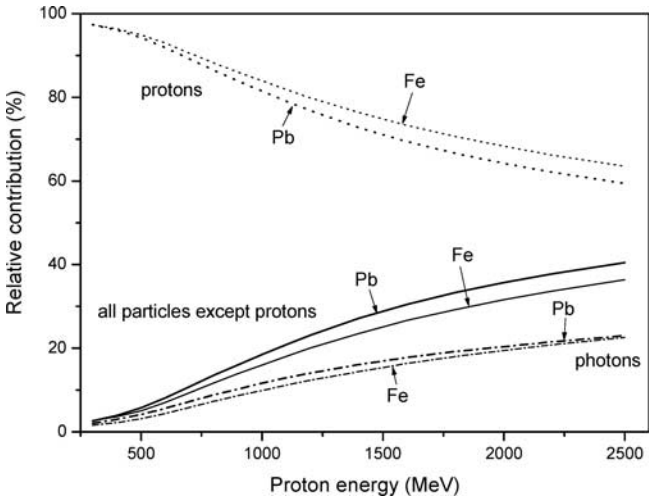

Fig. 23. Comparison of the relative contributions of different particles in the total heat deposition in the iron and lead targets irradiated with intermediate energy protons.

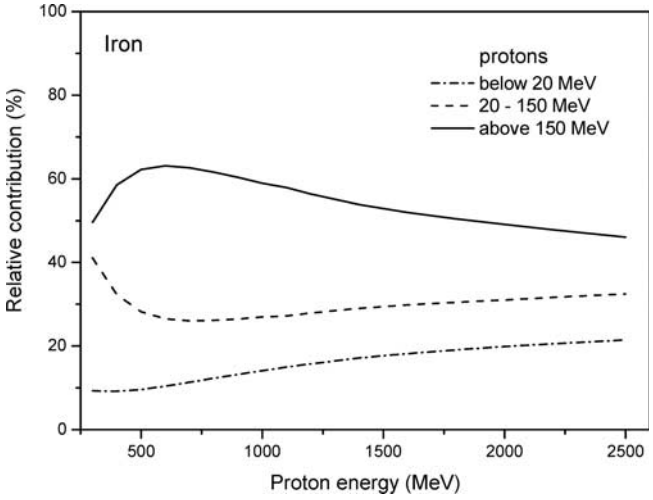

Fig. 24. Relative contribution of protons of different energies in the proton induced heat deposition in the iron target (R = 10 cm, H = 60 cm) irradiated with intermediate energy protons calculated with the help of the Bertini model (MCNPX).

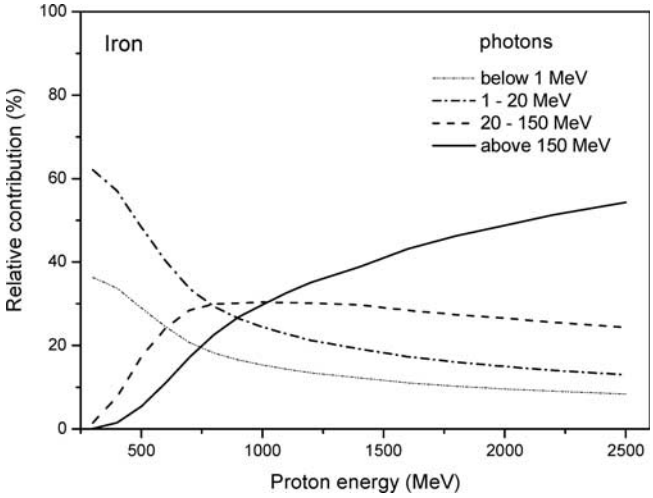

Fig. 25. Relative contribution of photons of different energies in the photon induced heat deposition in the iron target (R = 10 cm, H = 60 cm) irradiated with intermediate energy protons calculated with the help of the Bertini model (MCNPX).

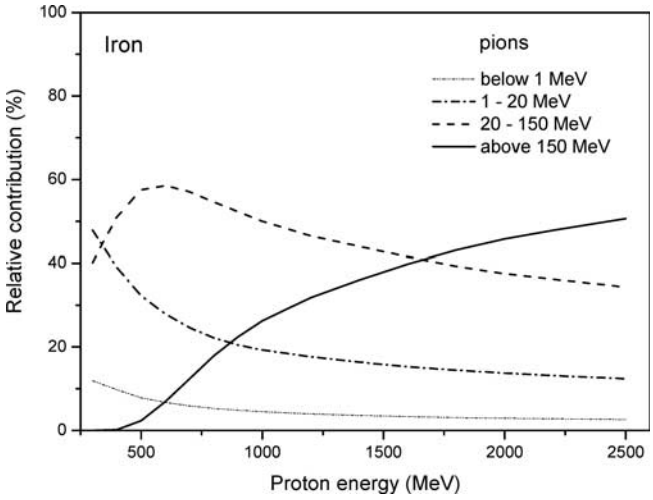

Fig. 26. Relative contribution of π^+ and π^- of different energies in the charged pion induced heat deposition in the iron target (R = 10 cm, H = 60 cm) irradiated with intermediate energy protons calculated with the help of the Bertini model (MCNPX).

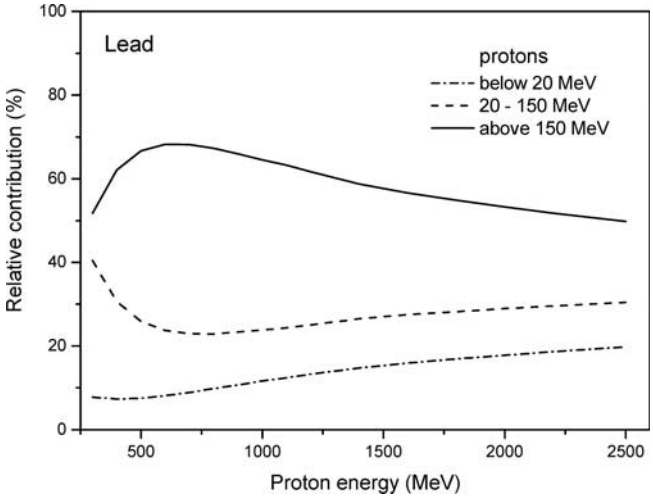

Fig. 27. Relative contribution of protons of different energies in the proton induced heat deposition in the lead target (R = 10 cm, H = 60 cm) irradiated with intermediate energy protons calculated with the help of the Bertini model (MCNPX).

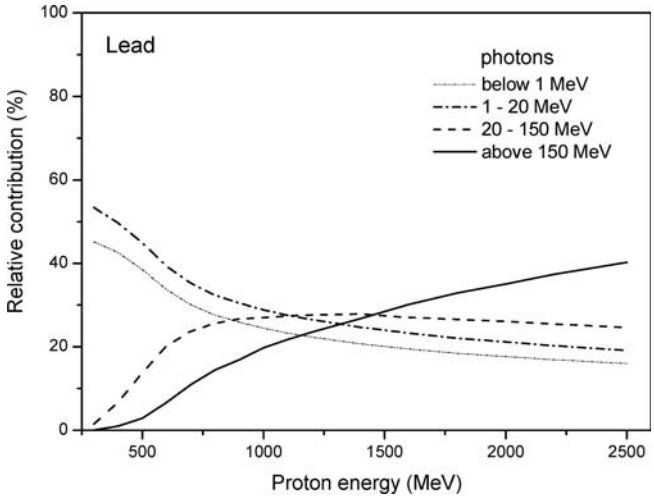

Fig. 28. Relative contribution of photons of different energies in the photon induced heat deposition in the lead target irradiated with intermediate energy protons calculated with the help of the Bertini model (MCNPX).

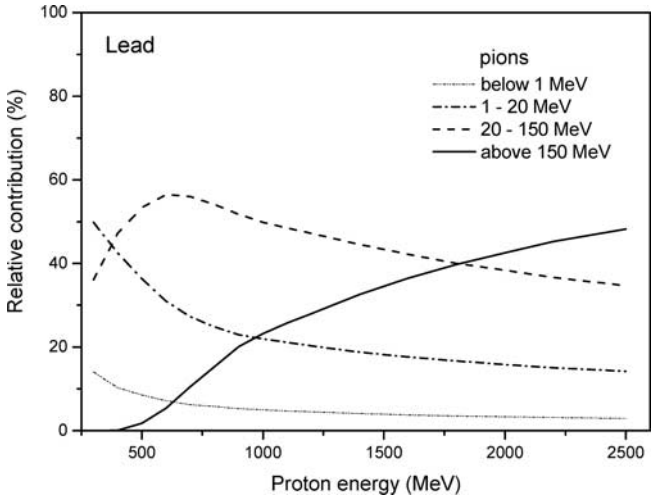

Fig. 29. Relative contribution of π^+ and π^- of different energies in the charged pion induced heat deposition in the lead target irradiated with intermediate energy protons calculated with the help of the Bertini model (MCNPX).

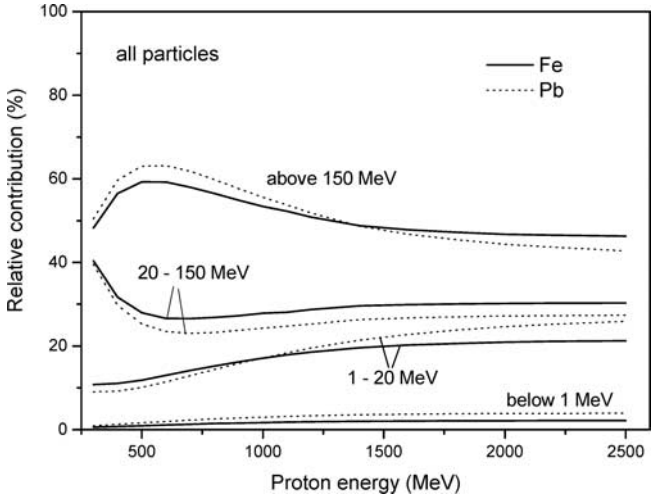

Fig. 30. Comparison of the relative contributions of the particles of different energies in the total heat deposition in the iron and lead target irradiated with intermediate energy protons calculated with the help of the Bertini model (MCNPX).

fixed energy ranges of particles, below 1 MeV, from 1 to 20 MeV, from 20 to 150 MeV and above 150 MeV to the total energy deposition due to the interactions of the considered particles with the target. The contribution of protons with the energy below 20 MeV is growing with the increase of the primary proton energy (Figs. 24 and 27). The contribution of the energy range from 20 to 150 MeV decreases up to ~ 700 MeV and slowly increases at higher energies. The contribution of protons with the energy above 150 MeV grows up to ~ 700 MeV and then decreases. For the photons and pions (Figs. 25, 26, 28, 29) the energy dependence of the contribution of different energy ranges differs from the protons. There is the constant decrease of the contribution of particles with the energy below 20 MeV. The region 20 to 150 MeV shows the maximum located at the different primary proton energy for iron and lead. The contribution of particles with the energy above 150 MeV rises steadily.

The relative contribution of the energy ranges for all particles is shown in Fig. 30 for the iron and lead target. Fig. 30 illustrates the increasing importance of the energy range below 150 MeV for the heat deposition calculations.

5 Conclusion

The energy deposition has been calculated for the targets from carbon to uranium irradiated with intermediate energy protons with the help of the Bertini model, the CEM model and the ISABEL model incorporated in the MCNPX code package and with the help of the CASCADE/INPE code.

The values obtained using the different models and codes are in a good agreement for the carbon, aluminum, copper, lead and bismuth target. For uranium the prediction of the CEM model is close to the CASCADE/INPE model and the values calculated using the Bertini model are close to the values obtained with the help of the ISABEL model.

The comparison with the available experimental data for the heat deposition for 0.8, 1.0 and 1.2 GeV protons has been performed. The good agreement is observed for copper, lead and bismuth target (Figs. 4–6, 15–20). The calculated values of the energy deposition are noticeably higher than the experimental data for the carbon target (Figs. 1, 9, 10) and lower for the iron target (Figs. 13 and 14). At the proton energy equal to 0.8 GeV the calculations underestimate the values of the heat deposition measured at the distance above the proton range in the targets (Figs. 13 and 15).

The ISABEL model describes the total heat depositions measured for the different targets in the best way (Table 1). At the same time the prediction power of the different models is rather similar (Table 1). The general trend of the calculated total energy deposition with the change of atomic number of the target is in the agreement with the experimental data, except the case of iron (Fig. 8).

The contribution of different particles and energy ranges in the energy depositions has been studied. The different models predict similar values of the relative contribution of the protons, photons and neutrons in the total heat deposition (Tables 2–5). The results show the significant importance of the energy range of the particles up to 150 MeV for the energy deposition calculations (Fig. 30).

It is expedient to perform a new set of heat deposition measurements to study the observed systematics in the dependency of atomic number Z and to clarify the difference with experimental data, especially for iron.

(Received on 6 October 2003)

References

1 *Hughes, H. G.; Egdorf, H. W.; Gallmeier, F. C.; Hendricks, J. S. et al.:* MCNPX™ User's manual, Version 2.4.0, September 2002, LA-CP-02-408

2 *Barashenkov, V. S.; Konobeyev, A. Yu.; Korovin, Yu. A.; Sosnin, V. N.:* CASCADE/ INPE code system. Atomic Energy 87 (1999) 742

3 *Belyakov-Bodin, V. I.; Kazaritsky, V. D.; Povarov, A. L.; Chuvilo, I. V.; Sherstnev, V. A.; Ado, J. M.; Azhgirey, I. L.; Mokhov, N. V.:* Calorimetric measurements and Monte Carlo analyses of medium-energy protons bombarding lead and bismuth targets. Nucl. Instr. Meth. Phys. Res. A295 (1990) 140

4 *Belyakov-Bodin, V. I. et al.:* Calorimetric measurements and Monte Carlo analyses of medium-energy protons bombarding uranium targets. Atomic Energy 70 (1991) 339

5 *Belyakov-Bodin, V. I.; Andreev, A. M.; Dubinsky, V. D.; Kazaritsky, V. D.; Povarov, A. L.; Chuvilo, I. V.; Sherstnev, V. A.:* Calorimetric measurements of medium-energy protons bombarding beryllium, carbon and aluminium targets. Nucl. Instr. Meth. Phys. Res. A314 (1992) 508

6 *Belyakov-Bodin, V. I.; Andreev, A. M.; Dubinsky, V. D.; Chuvilo, I. V.; Sherstnev, V. A.:* Heat deposition in targets bombarded by medium-energy protons. Nucl. Instr. Meth. Phys. Res. A335 (1993) 30

7 *Beard, C. A.; Belyakov-Bodin, V. I.:* Comparison of energy deposition calculations by the LAHET Code System with experimental results. Nucl. Sci. Eng. 119 (1995) 87.

8 *Chadwick, M. B.; Young, P. G.; Chiba, S.; Frankle, S. C.; Hale, G. M.; Hughes, H. G.; Koning, A. J.; Little, R. C.; MacFarlane, R. E.; Prael, R. E.; Waters, L. S.:* Cross-section evaluations to 150 MeV for Accelerator-Driven Systems and implementation in MCNPX. Nucl. Sci. Eng. 131 (1999) 293

9 *Briesmeister, J. F.* (Ed.): MCNP™ – A general Monte Carlo N-particle transport code, UC abc and UC 700, LA-13709-M, Iss. March 2000

10 *Bertini, H. W.:* Low-energy intranuclear cascade calculation. Phys.-Rev. 131 (1963) 1801

11 *Bertini, H. W.:* Intranuclear-cascade calculation of the secondary nucleon spectra from nucleon-nucleus interactions in the energy range 340 to 2900 MeV and comparisons with experiment. Phys.Rev. 188 (1969) 1711

12 *Yariv, Y.; Fraenkel, Z.:* Intranuclear cascade calculation of high-energy heavy-ion interactions. Phys.Rev. C20 (1979) 2227

13 *Yariv, Y.; Fraenkel, Z.:* Intranuclear cascade calculation of high energy heavy ion collisions: effect of interactions between cascade particles. Phys. Rev. C24 (1981) 488

14 *Chen, K.; Fraenkel, Z.; Friedlander, G.; Grover, J. R.; Miller, J. M.; Shimamoto, Y.:* VEGAS: A Monte Carlo simulation of intranuclear cascades. Phys. Rev. 166 (1968) 949

15 *Iljinov, A. S.:* A code for intranuclear cascade calculation in the energy range < 5 GeV", JINR Report B1-4-5478, Dubna, 1970

16 *Barashenkov, V. S.; Toneev, V. D.:* Interaction of high energy particles and nuclei with atomic nuclei, Moscow, Atomizdat, 1972

17 *Gudima, K. K.; Mashnik, S. G.; Toneev, V. D.:* Cascade-exciton model of nuclear reactions. Nucl. Phys. A401 (1983) 329

18 *Mashnik, S. G.:* Neutron-induced particle production in the cumulative and noncumulative regions at intermediate energies. Nucl. Phys. A568 (1994) 703

19 *Mashnik, S. G.; Peterson, R. J.; Sierk, A. J., Braunstein, M. R.:* Pion-induced transport of ■ mesons in nuclei. Phys. Rev. C61 (2000) 034601

20 *Konobeyev, A. Yu.; Korovin, Yu. A.:* Application of the intranuclear cascade evaporation model. Kerntechnik 63 (1998) 124

21 *Bertini, H. W.; Harp, G. D.; Bertrand, F. E.:* Comparisons of predictions from two intranuclear-cascade models with measured secondary proton spectra at several angles from 62 – and 39 – MeV protons on various elements. Phys. Rev. C10 (1974) 2472

22 *Barashenkov, V. S.; Kostenko, B. F.; Zadorogny, A. M.:* Time-dependent intranuclear cascade model. Nucl. Phys. A338 (1980) 413

23 *Barashenkov, V. S.; Le Van Ngok; Levchuk, L. G.; Musulmanbekov, Zh. Zh. et al.:* CASCADE – the code package for the simulation of nuclear processes induced by high energy particles and nuclei in gaseous and condensed matter. JINR Report, R2-85-173, Dubna, 1985

24 *Kozłowski, M.; Müller, H. H.; Wagner, R.:* Analyzing power and cross section of the ^{58}Ni, ^{90}Zr, ^{209}Bi (■, ^{3,4}He X) reactions in the continuum described by the coalescence model. Nucl. Phys. A420 (1984) 1

25 *Awes, T. C.; Poggi, G.; Gelbke, C. K.; Back, B. B.; Glagola, B. G.; Breuer, H.; Viola, V. E.:* Precompound emission of light particles in the reaction ^{16}O+^{238}U at 20 MeV/nucleon. Phys. Rev. C 24 (1981) 89

26 *Konobeyev, A. Yu.; Korovin, Yu. A.; Vecchi, M.:* Fission product yields in nuclear reactions induced by intermediate energy particles. Kerntechnik 64 (1999) 216

27 *Waters L. S.* (editor): MCNPX™ User's manual, Version 2.3.0, April 2002, LA-UR-02-2607

The authors of this contribution

Dr. *C. H. M. Broeders*, Institut für Reaktorsicherheit, Forschungszentrum Karlsruhe GmbH, 76344 Eggenstein-Leopoldshafen, Germany
e-mail: cornelis.broeders@irs.fzk.de
Dr. of Sci. *A. Yu. Konobeyev* and *A. A. Travleyev*, Institute of Nuclear and Power Engineering, 249020 Obninsk, Russia
e-mail: konobeev@irs.fzk.de; e-mail: travleev@irs.fzk.de